Superconducting NbN and $CaFe_{0.88}Co_{0.12}AsF$ studied by point-contact spectroscopy with a nanoparticle Au array

HPSTAR
1096-2020

Y. F. Wu,[1,*] A. B. Yu,[3,4,5,*] L. B. Lei,[3,4,6] C. Zhang,[3,4,5] T. Wang,[3,4,6] Y. H. Ma,[3,4,5] Z. Huang,[3,4,6] L. X. Chen,[3,4] Y. S. Liu,[7,8] C. M. Schneider,[7,8] G. Mu,[3,4,5] H. Xiao,[2] and T. Hu[1,†]

[1]*Beijing Academy of Quantum Information Sciences, Beijing 100193, China*
[2]*Center for High Pressure Science and Technology Advanced Research, Beijing 100094, China*
[3]*State Key Laboratory of Functional Materials for Informatics, Shanghai Institute of Microsystem and Information Technology, Chinese Academy of Sciences, Shanghai 200050, China*
[4]*CAS Center for Excellence in Superconducting Electronics (CENSE), Shanghai 200050, China*
[5]*University of Chinese Academy of Sciences, Beijing 100049, China*
[6]*School of Physical Science and Technology, ShanghaiTech University, Shanghai 201210, China*
[7]*Peter Gruenberg Institute PGI-6, Forschungszentrum Juelich, D-52425 Juelich, Germany*
[8]*Fakultät für Physik, Universität Duisburg-Essen, D-47057 Duisburg, Germany*

(Received 23 December 2019; revised manuscript received 9 April 2020; accepted 13 April 2020; published 4 May 2020)

The point-contact-spectroscopy measurement is a powerful method to detect the superconducting gap and the spin polarization of materials. However, it is difficult to get a stable and clean point contact by conventional techniques. In this work, we fabricate multiple point contacts by depositing Au nanoparticle arrays on the surface of a superconductor through an anodic aluminum oxide patterned shadow mask. We obtained the superconducting gaps of niobium nitride thin film (NbN, $T_c = 16$ K) and iron superconductors $CaFe_{0.88}Co_{0.12}AsF$ single crystals (Ca-1111, $T_c = 21.3$ K) by fitting the point-contact spectroscopy with the Blonder-Tinkham-Klapwijk theory. We found that NbN's gap (Δ) exhibits the BCS-like temperature dependence with $\Delta \approx 2.88$ meV at 0 K and $2\Delta/k_BT_c \approx 4.22$ in agreement with previous reports. By contrast, Ca-1111 has a multigap structure with $\Delta_1 \approx 1.99$ meV and $\Delta_2 \approx 5.01$ meV at 0 K, and the ratio between the superconducting gap and T_c is $2\Delta_1/k_BT_c = 2.2$ and $2\Delta_2/k_BT_c = 5.5$, suggesting an unconventional paring mechanism of Ca-1111 also in agreement with previous reports on other Fe-based superconductors. Our multiple point-contacts method thus provides an alternative way to perform measurements of the superconducting gap.

DOI: 10.1103/PhysRevB.101.174502

I. INTRODUCTION

Andreev reflection describes a transport process occurring at the interface between normal metals and superconductors [1]. In Andreev reflection, the electrons from the normal metal will be reflected back as a hole with opposite spin and velocity, but equal momentum allowing a charge transmission within the superconducting energy gap [1]. The Andreev reflection spectra is usually obtained by measuring the differential conductances of point contacts between metals and superconductors. By fitting the point-contact Andreev reflection (PCAR) spectra with the Blonder-Tinkham-Klapwijk (BTK) theory [2], one can obtain the fundamental properties of superconductors, such as the superconducting gap energy. Compared to the complex techniques such as angle-resolved photoemission spectroscopy and scanning tunneling microscopy, which require a large-scale and atomically flat surface of samples, the PCAR spectroscopy is a convenient and efficient tool to probe spectroscopic information of superconductors. Furthmore, PCAR spectra are also a powerful tool to study the spin polarization of metals in contact with a superconductor[3–7].

The key to obtain reliable PCAR spectroscopy results lies in the contact interface between normal metals and superconductors. The contact interface has to be clean, stable, and of small size, which has to be less than the electron mean free path in order to make a ballistic contact and to ensure the whole voltage drop occurring at the interface. Otherwise, no spectroscopic information or nonideal spectroscopic features will appear in the transport curves. Up to now, there are two typical techniques developed to fabricate the point-contact interface. One is the so-called needle-anvil technique, where the normal metal is a sharp needle fabricated by electrochemical and mechanical methods. This technique offers a controllable way to produce a single point contact by slowly pressing the needle to the surface of the superconductor in different positions controlled by a high-precision micromechanical device [4,8,9]. However, the needle-anvil technique has two major disadvantages: poor contact stability and hard to apply to a very small sample. The other one is the microbridge technique. The small conducting bridge between the normal metals and superconductors is created

*These authors contributed equally to this work.
†hutao@baqis.ac.cn

 ©2020 American Physical Society

artificially by lithography technology, electric breakdown, and a small drop of silver paste or a small indium flake, which provides a robust and thermally stable contact point [10–12]. The microbridge technique allows for conducting directional point-contact measurements even in a dilution refrigerator. But it has some disadvantages, such as the complex manufacturing process from the many lithographic fabrication steps and the uncontrollable conductive channels in the silver paste or indium flake. Despite the fact that the conductive channel can be modified by the application of short current or voltage pulses, the electric breakdown might ruin the surface of ultrathin superconductors.

In this paper, we present a method to perform point-contact measurements with robust, clean, and easily obtained point contacts. The multiple point contacts are fabricated by depositing nanoscale Au onto the superconductors through an anodic aluminum oxide (AAO) patterned shadow mask. It is found that the interface size between Au and NbN is close to the hole size of the AAO mask and there is no significant interface contamination between them. These parallel nanometric channels connecting samples allow for voltage drop occurring at the interface, which makes the energy-resolved information available. These measurements are carried out under various temperatures and various magnetic fields, and are analyzed by the BTK theory. The obtained superconducting gap of NbN films exhibits a BCS-like temperature dependence with the gap energy about 2.88 meV at 0 K in good agreement with previous reports for 50-nm NbN films [13,14]. With the same method, $CaFe_{0.88}Co_{0.12}AsF$ (Ca-1111) was found to be a multigap superconductor with two energy gaps as usually observed in iron-based superconductors [15–18]. Both gaps, $\Delta_1 \approx 1.99$ meV and $\Delta_2 \approx 5.01$ meV at 0 K with the ratios $2\Delta_1/k_BT_c = 2.2$ and $2\Delta_2/k_BT_c = 5.5$, respectively, show BCS-like temperature-dependent behavior. In addition, the ratio of gaps $\Delta_2(0)/\Delta_1(0)$ has the value near to 3, suggesting that an unconventional pairing mechanism may exist in Ca-1111. Furthermore, this method also provides a possible way to investigate the spin polarization of materials by depositing superconductor islands on the surface of a ferromagnet.

II. EXPERIMENTS

Figure 1 shows the fabrication process for multiple point-contact devices. The nano-Au array was synthesized by using thermal evaporation through a nanoporous AAO mask attaching to a superconductor sample. The commercially purchased AAO films were chosen to be the mask of the nanoarray. Its pore diameter is 50 nm, interpore distance is 100 nm, and thickness is about 200 nm. We chose a piece of film with the size of 1 mm × 1 mm for the present experiment. First, the AAO film was placed in acetone to remove the residual polymethyl methacrylate left over from production. Subsequently, it was taken out and placed in a fume hood to dry naturally to prevent it from breaking. And then, it was slowly placed onto the superconductor. The adhesion to the sample arises from electrostatic forces. After doing this, the nano-Au array would be grown on them by thermal deposition in a high-vacuum environment no less than 10^{-5} Pa. The rate of Au deposition is monitored by the film thickness

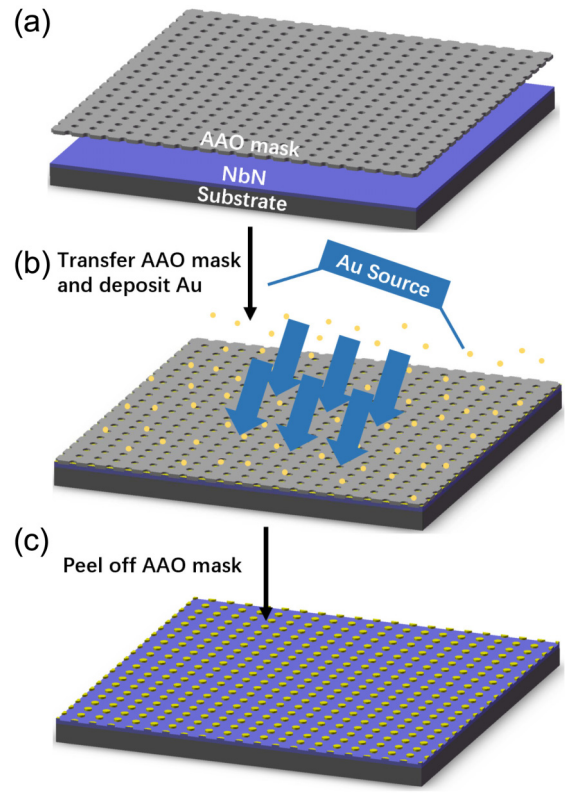

FIG. 1. The fabrication process for multiple point-contact devices. (a) The nanoporous anodic aluminum oxide (AAO) mask is placed on top of NbN thin film. (b) The Au arrays are grown on NbN by using thermal vapor deposition via the AAO mask. (c) The obtained regular Au nanoarray structure.

gauge and should not exceed 0.1 Å per second to prevent the clogging of the AAO pores. The final thickness of the Au film is approximately 50 nm. After taking out the sample from the thermal deposition chamber, we start to remove the covered AAO mask from the sample. The AAO mask can be taken down by a low-viscosity tape. Such a process is like mechanical exfoliation of epitaxial graphene, which will not damage the deposited array on the surface of superconductor samples. Finally, we can get a regular Au nanoarray structure as shown in Fig. 1(c).

The NbN samples consist of 50-nm NbN films grown through reactive magnetron sputtering on single-crystal MgO(100) substrates (0.5 cm × 0.5 cm) [19]. The high-quality Ca-1111 single crystal was grown by a self-flux method with CaAs as the flux [20,21] and the amount of Co doping is determined to be 0.12, as measured by energy dispersive x ray). The *ab*-plane area of the crystal is about 1 mm^2 and the thickness is about 50 μm or less. We made the top contact over the nano-Au array by an Ag-paint spot. During this process, a slightly dry Ag-paste drop is chosen, which helps to prevent Ag paste from permeating into the empty spaces between Au islands. In addition, we have tried to apply Ag paste to the deposited gold without removing the AAO mask. We found no significant difference between point-contact spectra with and without the AAO mask. It thus

suggests that the contact with the sample surface is made through the Au nanoparticles. Most of the time the AAO mask has to be removed from the sample, since it is usually hard to contact the Au nanoparticle through the hole of the AAO mask for producing a current path.

III. RESULTS AND DISCUSSION

The obtained nano-Au array on the surface of NbN has a relatively high degree of order as shown in scanning electron microscopy (SEM) in Fig. 2(a). It is worth noticing that the real nanohole array on the AAO mask is not so periodic as that shown in the sketch plot in Fig. 1. This is because the AAO mask may become wrinkled or crumpled during the process of transferring the mask onto the sample. Thus, the distribution of Au nanoparticles has a relatively high degree of order. The tight attachment of the AAO mask to the NbN film is the key parameter to guarantee a nice array structure since the vibration during the thermal deposition will smear the array structure. The atomic force microscope (AFM) image in Fig. 2(b) shows each Au island has roughly the same size and the diameter of the island is close to 80 nm. Figure 2(c) is the transmission electron microscope (TEM) of the cross section of the sample. It is shown in Fig. 2(c) that the interface size between Au and NbN is approximately 50 nm close to the hole size of AAO mask and there is no significant interface contamination. These results suggest that depositing metal through the AAO mask indeed provides a reliable and nondamaging method, which is an advantage especially for some unstable samples. Thus, these point-contact measurements can be performed in a moderate vacuum, high magnetic field or ultralow temperature environments without requiring the sample to be flat at the atomic level. It may also be applicable to an ultrathin superconductor film, like the mechanically exfoliated superconductors, which usually has a small and fragile surface. Furthermore, the technique is more flexible for the point-contact study. For example, one can deposit superconductor islands on the surface of ferromagnets to investigate the spin polarization of charge carriers of samples.

The inset of Fig. 3 shows the current configuration for multiple point-contact transport measurements, where the Au islands are used as the metal bridges, which connect with the superconductor in parallel. Despite a macroscopic electric contact, the metal/superconductor contact is really made up of nano point-contact units by controlling the size and spacing of the islands through the AAO mask. A small point contact between metal and superconductor is a necessary condition to Andreev reflection measurements. Only if the metal size is smaller than the mean free path, electrons move ballistically and tunnel to another material through this point [22], which makes the energy-resolved information available [18]. Generally, the smaller the contact area, the less inelastic the scattering configurations and the greater the intensity of the spectroscopic signal. It is worth noticing that the real contact area is usually less than the pore size of AAO masks, because of the roughness of superconductor surfaces.

Thus we can, in principle, restrict the real contact area to any extent by choosing AAO masks with different pore sizes, since the real contact area of every nanoparticle is limited by the pore area. For a superconductor sample with rough surfaces, the real contact area is expected to be much less than the pore size of AAO masks, while for a flat sample the contact area has almost the same size as the AAO mask, as shown in Fig. 2(c). Thus, in contrast to a small metal bridge made by

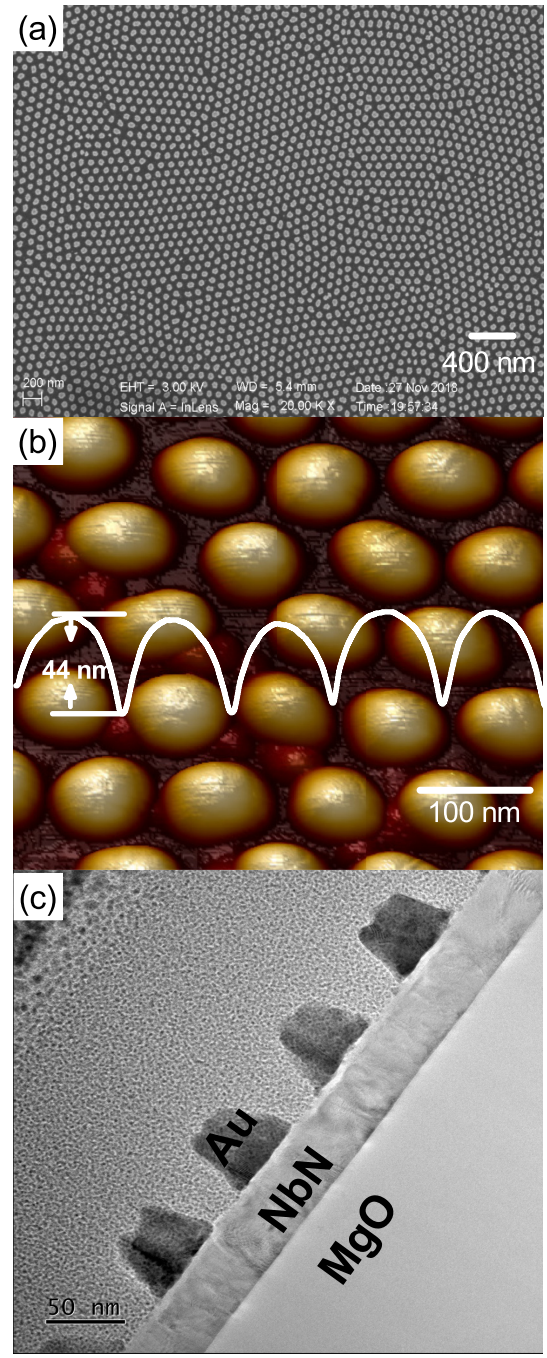

FIG. 2. Characterization of the nano-Au array/NbN structure. (a) The SEM image of the Au array on NbN film. Scale bar is 400 nm. (b) The AFM image of a smaller range of the Au array. Scale bar is 100 nm. The white curve shows the measurements of the islands' height and width. (c) TEM image of the cross section of the Au/NbN heterojunction. Scale bar is 50 nm. From the lower right to the top left corner are the MgO_2 substrate, 50 nm NbN, Au array, and gold surface coating prior to focused ion beam processing, respectively.

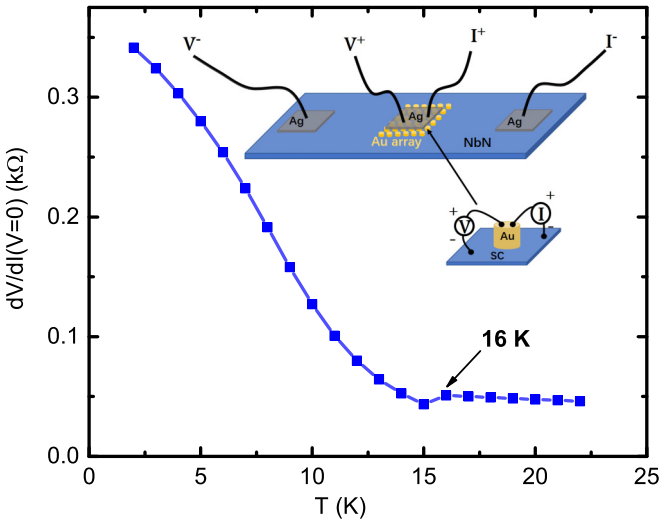

FIG. 3. The temperature dependence of differentiate resistance at zero-bias voltage. The inset shows a schematic structure of the measurement configuration for electrical transport in the nano-Au array/NbN structure and the circle shows point contact from one Au island.

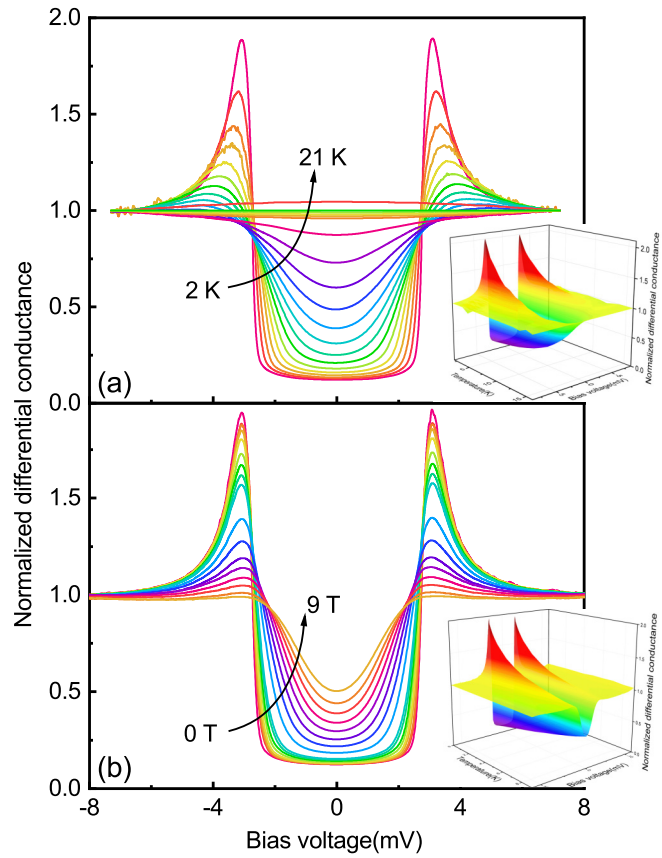

FIG. 4. Temperature (T) and magnetic field (H) dependence of tunneling spectroscopy of NbN film in the metal-array/superconductor structure. (a) Temperature (from 2 to 21 K with the step of 1 K) evolution of the normalized conductance curve of 50-nm NbN film measured at 0 T. (b) magnetic field (from 0 to 1 T with the step of 0.2 T and from 1 to 9 T with the step of 1 T) evolution of the normalized conductance curve of 50-nm NbN film at 2 K. The inset is the three-dimensional view of tunneling conductance measured by the point-contact structure at different temperatures and magnetic fields.

the very complicated etching or photolithography process [5], the size of the contact here can be controlled by changing the AAO masks which usually meet the requirements for PCAR spectroscopy measurements. Furthermore, in the multicontact structure, the superconducting coherence peak may not be as sharp as that from the single point method. Ths is because the PCAR spectroscopy in a multicontact structure is an average result of array points, where the different properties from different areas of an inhomogeneous sample will result in a different superconducting energy gap and the consequent PCAR spectroscopy [23].

The main plot of Fig. 3 shows the temperature dependence of the differential resistance for 50-nm NbN film at zero-bias voltage by using the multiple point-contact method. The differential resistance values are measured by the electrical transport option in a physical property measurement system from Quantum Design. The resistance shows a drop at 16 K, but an increase again upon further cooling down. The drop of resistance at 16 K is due to the superconducting transition of the NbN [24]. The increase of resistance at low temperature is widely observed in normal metal–superconductor junctions at very low temperature and bias voltage is due to opening of the NbN gap and freezing out of subgap conductance.

Figure 4(a) shows the normalized differential conductances $[dI/dV(T)/dI/dV(16\ \mathrm{K})]$ versus direct current (DC) bias. The normalized differential conductances exhibit superconducting coherence peaks just below $T = 13$–14 K, where the differential conductances are normalized to the value at the superconducting critical temperature $T_c = 16$ K. According to the position of the coherence peaks, the superconducting energy gap at 2 K and 0 T is estimated to be 2.88 meV, which is consistent with the superconducting energy gap of bulk NbN measured by scanning tunneling spectroscopy or other PCAR methods [13,14]. The coherence peak is sharp at 2 K while shrinking gradually with temperature and becoming flat above 13–14 K as shown in the three-dimensional plot of the differentiate conductance-bias voltage temperature in the inset of Fig. 4(a). The coherence peak can be also suppressed by the applied field (H) as shown in Fig. 4(b).

The obtained differential conductance spectra is further analyzed within the BTK model [2]. The red line in Fig. 5(a) is the best fitting curve to the differential conductance spectra at 2 K and 0 T. The fitting parameters are $Z = 2.13$, $\Gamma = 0.27$ meV, and $\Delta = 2.89$ meV, where Z, Γ, and Δ describe the transparency of the interface, the intrinsic and extrinsic sources of the finite lifetime, and the superconducting gap, respectively. The value of Z is much larger than 1, which suggests that the point-contact spectra are in the tunneling regime. This result can be understood as follows: the oxide barrier at NbN surfaces acts as a tunnel barrier, which usually forms once NbN films are exposed to air.

In addition, the fitting result of $\Delta = 2.89$ meV is consistent with the value of the gap (2.88 meV) estimated from the superconducting coherence peaks, which is usually expected

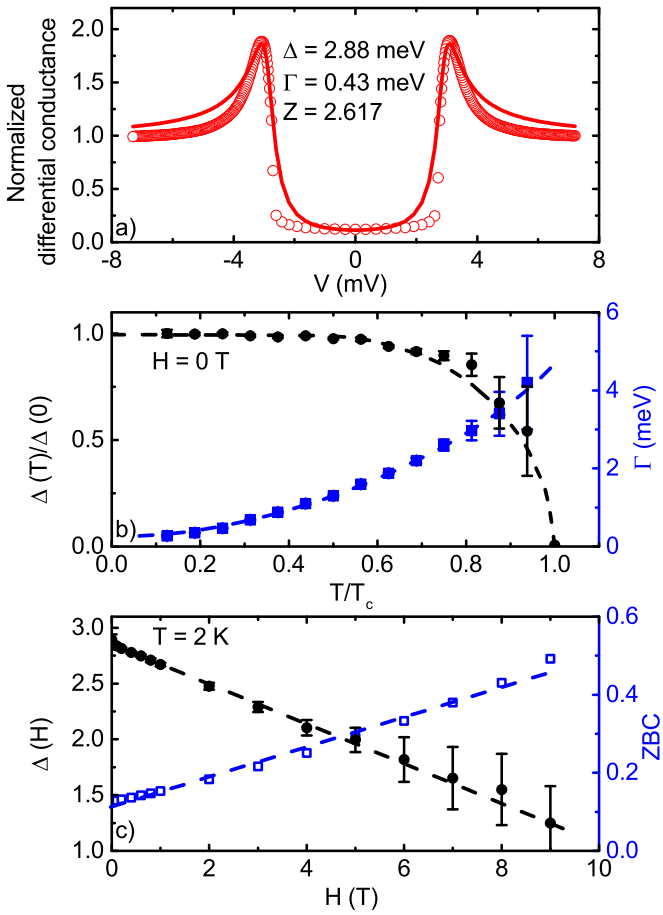

FIG. 5. Superconducting energy gap. (a) The normalized PCAR spectra of 50-nm NbN film at 2 K (red open dots) with the best fitting result (red line) by the modified BTK model ($Z = 2.13$, $\Gamma = 0.27$ meV, and $\Delta = 2.89$ meV). (b) The temperature dependence of the superconducting energy gap (left axis, black dots) normalized by the value at $T = 0$ K and the broadening parameters (Γ) (right axis, blue solid square) given by the BTK fit with a dashed line as a guide to the eye. The black dashed line shows the temperature dependence of the magnitude of the superconducting gap determined by BCS theory. (c) The magnetic field dependence of the superconducting gap (left axis) and the zero-bias normalized differential conductance (ZBC) (right axis) at 2 K. The black dashed line is the linear fitting curve to the Δ and the blue dashed line is the linear fitting curve to the ZBC.

when Z is large and Γ is small. The similar value of gap was also observed in several other samples as shown in the Supplemental Material, which shows the reproducibility of the data [25]. To investigate the superconducting properties of the NbN film, we summarize the data of the superconducting energy gap at different temperatures in the main plot of Fig. 5(b). When we fit the PCAR spectra at different temperature, the parameter Z is fixed at 2.1–2.2. It is worth noting that for a tunneling junction ($Z > 1$), the Δ and Γ obtained in the BTK model are essentially independent of Z. As the temperature increases, the superconducting gap gradually decreases in the low-temperature range, but shows a fast drop near T_c, suggesting a BCS-like gap behavior of NbN [26]. The $\Delta(T)$ variation can be fitted by a BCS curve, which gives the ratio $2\Delta(0)/k_B T_c = 4.22$ as shown in Fig. 5(b). The value of 4.22 is larger than the BCS ratio of 3.52 suggesting a strong electron-phonon coupling in NbN [26]. And as shown in Fig. 5(b), the value of Γ (blue solid square) increases with increasing temperature. The superconducting gap is also suppressed by magnetic field, showing a monotonic decrease with the increase of the magnetic field at 2 K as in Fig. 5(c). For the sake of emphasizing the new point-contact technique, we simplify the analysis by using a simple single-band BTK function to fit the point-contact spectra in magnetic field and obtain the superconducting gap instead of using the fitting equation in Ref. [27]. In addition, the magnetic field has a strong influence on the zero-bias normalized differential conductance that increases with the increase of magnetic field. Interestingly, a linear fitting to the ZBC at 2 K gives the value of 1 at 25 T, which is consistent with the previous reports of the upper critical magnetic field H_{c2} for NbN thin films [28]. A possible explanation for the linear behavior of the ZBC is that the junction area could be seen as a mixture of normal regions (vortex cores) and superconducting ones, where the increasing zero-bias tunneling conductance is proportional to the increasing volume fraction of vortex cores and consequently shows a linear dependence on the applied magnetic field [29,30].

The superconducting energy gap of Ca-1111 was also investigated through the multiple point-contact measurements and we analyzed these spectra as shown in Fig. 6. We found that the resistance of Ca-1111 is almost linear above T_c and decreases suddenly at $T_c \approx 21.3$ K as shown in the inset to Fig. 6(a). The main plot in Fig. 6(a) shows the single-crystal Ca-1111 normalized differential conductances vs DC bias at temperatures 2–19 K with zero field, which are normalized to the value at normal state (30 K). There are two superconducting coherence peaks below the temperature $T = 7$ K, which are suppressed by the increasing temperature and merge into one peak. An unsymmetrical behavior can be found in it. This unsymmetrical appearance is common to most point-contact and tunneling spectroscopy measurements, which may be related to the rapid decrease in the density of states upon crossing the Fermi level [31,32]. The shape of the spectra is similar to the double-gap structure of $Ba(Fe_{1-x}Co_x)_2As_2$ [33] and $SmFeAsO_{1-x}F_x$ [17]. Thus we fit the data using the two-gap BTK model [8] $G = w_1 G_1^{\mathrm{BTK}} + (1 - w_1) G_2^{\mathrm{BTK}}$, where w_1 is the weight of band 1. The two conductances G_1^{BTK} and G_2^{BTK} depend on gap values Δ_1 and Δ_2, broadening parameters Γ_1 and Γ_2 and barrier parameters Z_1 and Z_2. Typical fitting results are given as the solid lines in Fig. 6(a).

Almost constant (small change of the order of 20%) barrier parameters $Z_1 = 0.42$, $Z_2 = 0.41$ and the weight factor $w_1 = 0.6 \pm 0.03$ are used for fitting conductance curves. Note that the fitting parameters of Ca-1111 $Z_1 = 0.42$ and $Z_2 = 0.41$ are much smaller than 1. In principle, the dimensionless effective barrier parameter Z represents an approximation of the complex underlying physics of the interface [34]. If the Z value is much lower than 1, ballistic Andreev reflection will occur at the contact interface and the energy-resolved information collected by point-contact measurement will be reliable [35]. The temperature dependence of the broadening parameters (Γ_1 and Γ_2) and gaps (Δ_1 and Δ_2) are also shown in Figs. 6(b) and 6(c). Γ_1 and Γ_2 practically keep

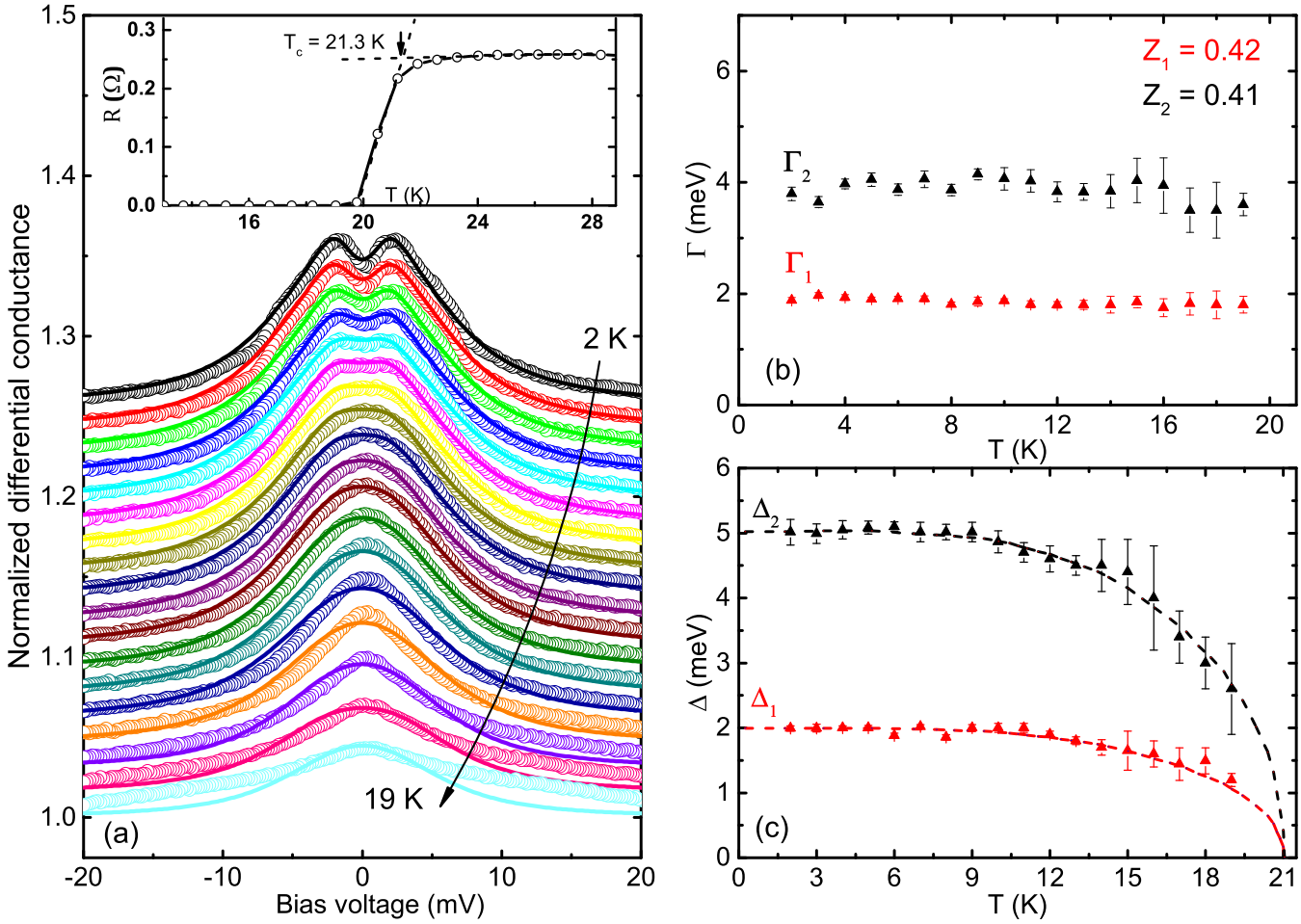

FIG. 6. The PCAR spectroscopy and superconducting gap of $CaFe_{0.88}Co_{0.12}AsF$. (a) Normalized conductance curves (symbols) of Au-$CaFe_{0.88}Co_{0.12}AsF$ measured from 2 to 19 K with the step of 1 K under zero field. The solid lines are given by a two-gap BTK model. Inset: The temperature dependence of resistance. (b) and (c) show the temperature dependence of the broadening parameters (Γ_1 and Γ_2) and gaps (Δ_1 and Δ_2).

constant with the increasing of temperature, which is similar to $SmFeAsO_{0.91}F_{0.09}$ [17]. The gaps function of temperature is BCS-like, with $\Delta_1(0) = 1.99$ meV and $\Delta_2(0) = 5.01$ meV, that is, $2\Delta_1(0)/k_BT_c = 2.2$ and $2\Delta_2(0)/k_BT_c = 5.5$. Here, the error bars are defined as the uncertainty due to the fit. Similar results were also observed in other $CaFe_{0.88}Co_{0.12}AsF$ samples as shown in the Supplemental Material [25].

Interestingly, the ratio of two gaps $\Delta_2(0)/\Delta_1(0) \approx 3$, was also reported in other iron-based superconductors such as $SmFeAsO_{1-x}F_x$, $LaFeAsO_{1-x}F_x$, and $Ba_{0.55}K_{0.45}Fe_2As_2$ [16,17,36,37]. The high value of the gap ratio $\Delta_2(0)/\Delta_1(0)$ was interpreted as the consequence of a $s\pm$ wave superconductor with nodeless and opposite sign order parameters caused by a spin-fluctuation mediated pairing mechanism [38,39]. Thus, it suggests that an unconventional pairing mechanism may exist in Ca-1111, which shows most likely the $s\pm$ wave symmetry.

IV. CONCLUSIONS

In summary, the nano-Au array point-contact structure has been successfully fabricated by using the AAO mask. The superconducting energy gap of 50 nm NbN film is determined to be about 2.88 meV at 0 K and shows a BCS-like temperature-dependent behavior in agreement with the previous reports. With the same method, Ca-1111 shows a multigap behavior, and the obtained two gaps are $\Delta_1 \approx 1.99$ meV and $\Delta_2 \approx 5.01$ meV at 0 K. The ratios of $2\Delta_1/k_BT_c = 2.2 < 3.52$ and $2\Delta_2/k_BT_c = 5.5 > 3.52$ suggest that an unconventional pairing mechanism exists in Ca-1111. Our multiple point-contact method thus provides a way to probe the superconducting gap.

ACKNOWLEDGMENTS

The authors acknowledge the support of National Natural Science Foundation of China Grant No. 11574338, National Natural Science Foundation of China–China Academy of Engineering Physics NSAF Joint Fund Grant No. U1530402, and China Postdoctoral Science Foundation Grants No. 2019T120366 and No. 2019M651620.

[1] A. Andreev, Sov. Phys. JETP **46**, 5 (1964).

[2] G. E. Blonder, M. Tinkham, and T. M. Klapwijk, Phys. Rev. B **25**, 4515 (1982).

[3] M. J. M. de Jong and C. W. J. Beenakker, Phys. Rev. Lett. **74**, 1657 (1995).

[4] R. Soulen, J. Byers, M. Osofsky, B. Nadgorny, T. Ambrose, S. Cheng, P. R. Broussard, C. Tanaka, J. Nowak, J. Moodera *et al.*, Science **282**, 85 (1998).

[5] S. K. Upadhyay, A. Palanisami, R. N. Louie, and R. A. Buhrman, Phys. Rev. Lett. **81**, 3247 (1998).

[6] G. J. Strijkers, Y. Ji, F. Y. Yang, C. L. Chien, and J. M. Byers, Phys. Rev. B **63**, 104510 (2001).

[7] Y. Ji, G. J. Strijkers, F. Y. Yang, C. L. Chien, J. M. Byers, A. Anguelouch, G. Xiao, and A. Gupta, Phys. Rev. Lett. **86**, 5585 (2001).

[8] P. Szabo, P. Samuely, J. Kačmarčík, T. Klein, J. Marcus, D. Fruchart, S. Miraglia, C. Marcenat, and A. G. M. Jansen, Phys. Rev. Lett. **87**, 137005 (2001).

[9] Y. G. Naidyuk, J. G. Najdjuk, and I. Yanson, *Point-Contact Spectroscopy* (Springer Science & Business Media, Berlin, 2005), Vol. 145.

[10] R. S. Gonnelli, D. Daghero, G. A. Ummarino, V. A. Stepanov, J. Jun, S. M. Kazakov, and J. Karpinski, Phys. Rev. Lett. **89**, 247004 (2002).

[11] R. S. Gonnelli, D. Daghero, D. Delaude, M. Tortello, G. A. Ummarino, V. A. Stepanov, J. S. Kim, R. K. Kremer, A. Sanna, G. Profeta, and S. Massidda, Phys. Rev. Lett. **100**, 207004 (2008).

[12] W. Dai, A. Richardella, R. Du, W. Zhao, X. Liu, C. Liu, S.-H. Huang, R. Sankar, F. Chou, N. Samarth *et al.*, Sci. Rep. **7**, 7631 (2017).

[13] H. Le Duc, W. Kaiser, and J. Stern, Appl. Phys. Lett. **50**, 1921 (1987).

[14] D. Hazra, N. Tsavdaris, S. Jebari, A. Grimm, F. Blanchet, F. Mercier, E. Blanquet, C. Chapelier, and M. Hofheinz, Supercond. Sci. Technol. **29**, 105011 (2016).

[15] T. Wang, Y. Ma, W. Li, J. Chu, L. Wang, J. Feng, H. Xiao, Z. Li, T. Hu, X. Liu *et al.*, npj Quantum Mater. **4**, 33 (2019).

[16] R. S. Gonnelli, D. Daghero, M. Tortello, G. A. Ummarino, V. A. Stepanov, J. S. Kim, and R. K. Kremer, Phys. Rev. B **79**, 184526 (2009).

[17] D. Daghero, M. Tortello, R. S. Gonnelli, V. A. Stepanov, N. D. Zhigadlo, and J. Karpinski, Phys. Rev. B **80**, 060502(R) (2009).

[18] D. Daghero and R. Gonnelli, Supercond. Sci. Technol. **23**, 043001 (2010).

[19] A. Shoji, S. Kiryu, and S. Kohjiro, Appl. Phys. Lett. **60**, 1624 (1992).

[20] Y. Ma, K. Hu, Q. Ji, B. Gao, H. Zhang, G. Mu, F. Huang, and X. Xie, J. Cryst. Growth **451**, 161 (2016).

[21] Y. Ma, H. Zhang, B. Gao, K. Hu, Q. Ji, G. Mu, F. Huang, and X. Xie, Supercond. Sci. Technol. **28**, 085008 (2015).

[22] W. McMillan, Phys. Rev. **175**, 537 (1968).

[23] V. Baltz, A. Naylor, K. Seemann, W. Elder, S. Sheen, K. Westerholt, H. Zabel, G. Burnell, C. Marrows, and B. Hickey, J. Phys.: Condens. Matter **21**, 095701 (2009).

[24] B. Matthias, Phys. Rev. **92**, 874 (1953).

[25] See Supplemental Material at http://link.aps.org/supplemental/10.1103/PhysRevB.101.174502 for the PCAR spectrum of other NbN and $CaFe_{0.88}Co_{0.12}AsF$ samples.

[26] K. Komenou, T. Yamashita, and Y. Onodera, Phys. Lett. A **28**, 335 (1968).

[27] P. Szabó, P. Samuely, Z. Pribulová, M. Angst, S. Bud'ko, P. C. Canfield, and J. Marcus, Phys. Rev. B **75**, 144507 (2007).

[28] M. Mathur, D. Deis, and J. Gavaler, J. Appl. Phys. **43**, 3158 (1972).

[29] P. Szabó, J. Girovský, Z. Pribulová, J. Kačmarčík, T. Mori, and P. Samuely, Supercond. Sci. Technol. **26**, 045019 (2013).

[30] M. Šindler, R. Tesař, J. Koláček, P. Szabó, P. Samuely, V. Hašková, C. Kadlec, F. Kadlec, and P. Kužel, Supercond. Sci. Technol. **27**, 055009 (2014).

[31] T. Chen, Z. Tesanovic, R. Liu, X. Chen, and C. Chien, Nature (London) **453**, 1224 (2008).

[32] R. Gonnelli, M. Tortello, D. Daghero, G. Ummarino, V. Stepanov, and J. Kim, Open Phys. **7**, 251 (2009).

[33] M. Tortello, D. Daghero, G. A. Ummarino, V. A. Stepanov, J. Jiang, J. D. Weiss, E. E. Hellstrom, and R. S. Gonnelli, Phys. Rev. Lett. **105**, 237002 (2010).

[34] K. Xia, P. J. Kelly, G. E. W. Bauer, A. Brataas, and I. Turek, Phys. Rev. B **65**, 220401(R) (2002).

[35] F. Magnus, K. Yates, S. Clowes, Y. Miyoshi, Y. Bugoslavsky, L. Cohen, A. Aziz, G. Burnell, M. Blamire, and P. Josephs-Franks, Appl. Phys. Lett. **92**, 012501 (2008).

[36] P. Szabó, Z. Pribulová, G. Pristáš, S. Bud'ko, P. C. Canfield, and P. Samuely, Phys. Rev. B **79**, 012503 (2009).

[37] S. Kawasaki, K. Shimada, G. F. Chen, J. L. Luo, N. L. Wang, and G.-Q. Zheng, Phys. Rev. B **78**, 220506(R) (2008).

[38] L. Benfatto, M. Capone, S. Caprara, C. Castellani, and C. Di Castro, Phys. Rev. B **78**, 140502(R) (2008).

[39] I. I. Mazin, D. J. Singh, M. D. Johannes, and M.-H. Du, Phys. Rev. Lett. **101**, 057003 (2008).